Inorganic Chemistry

Article

pubs.acs.org/IC

Computational Insights into Uranium Complexes Supported by Redox-Active α-Diimine Ligands

Giovanni Li Manni,[†] Justin R. Walensky,[‡] Steven J. Kraft,[⊥] William P. Forrest,[⊥] Lisa M. Pérez,[§] Michael B. Hall,*[,§] Laura Gagliardi,*[,∥] and Suzanne C. Bart*[,⊥]

[†]Department of Physical Chemistry, University of Geneva, Switzerland, CH-1211

[‡]Department of Chemistry, University of Missouri, Columbia, Missouri 65211, United States

[§]Department of Chemistry, Texas A&M University, College Station, Texas 77842, United States

[∥]Department of Chemistry and Supercomputing Institute, University of Minnesota, 207 Pleasant St. SE, Minneapolis, Minnesota 55455, United States

[⊥]Department of Chemistry, Purdue University, West Lafayette, Indiana 47907, United States

Supporting Information

ABSTRACT: The electronic structures of two uranium compounds supported by redox-active α-diimine ligands, $(^{Mes}DAB^{Me})_2U(THF)$ (**1**) and $Cp_2U(^{Mes}DAB^{Me})$ (**2**) ($^{Mes}DAB^{Me}$ = [ArN=C(Me)C(Me)=NAr]; Ar = 2,4,6-trimethylphenyl (Mes)), have been investigated using both density functional theory and multiconfigurational self-consistent field methods. Results from these studies have established that both uranium centers are tetravalent, that the ligands are reduced by two electrons, and that the ground states of these molecules are triplets. Energetically low-lying singlet states are accessible, and some transitions to these states are visible in the electronic absorption spectrum.

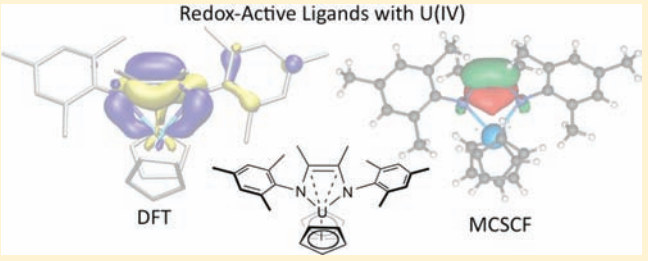

INTRODUCTION

Redox-active ligands are becoming popular for use in organometallic chemistry because of their ability to stabilize reactive metal centers.[1] However, these ligands create ambiguous metal oxidation states;[2] thus, multiple characterization techniques[3] must be used to establish the electronic structures of these complexes. Ligand oxidation states can be determined by examining geometric distortions obtained from the molecular structure, which in turn helps to assign the metal oxidation state.[3] Comparison of this experimental data with geometry optimizations obtained from density functional theory (DFT) allows creation of an accurate model. Further computations based on multiconfigurational self-consistent field (MCSCF) methods are useful to accurately determine the ground state and low-lying excited states often present in systems with these types of complicated redox non-innocent frameworks.[3−5]

Both DFT methods and MCSCF calculations were performed to further probe the electronic structures of two uranium compounds supported by redox-active α-diimine ligands, $(^{Mes}DAB^{Me})_2U(THF)$ (**1**) and $Cp_2U(^{Mes}DAB^{Me})$ (**2**) ($^{Mes}DAB^{Me}$ = [ArN=C(Me)C(Me)=NAr]; Ar = 2,4,6-trimethylphenyl (Mes)) (Figure 1).[6] Although formally "U(0)" and "U(II)", respectively, characterization by X-ray absorption spectroscopy (XAS) indicates that these species contain tetravalent uranium centers, a formulation made possible by invoking two-electron reduction of each α-diimine ligand to form ene−diamide frameworks.[3a,6,7] The redox-active nature of the ligand is supported by both electronic absorption spectroscopy, which shows characteristic f−f transitions expected for uranium(IV), and X-ray crystallography, which shows the expected bond distortions associated with occupation of the ligand π* orbitals.[3a,6,7] Herein, we report the results of this computational study, which confirm the redox-active nature of the ligands, establish the uranium centers as tetravalent, and determine the ground and excited states. Further analyses by complete active space state interaction

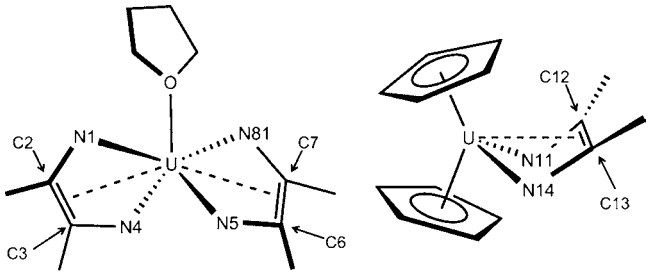

Figure 1. Molecules used for computational study. Aryl groups have been truncated for clarity.

Received: August 5, 2011
Published: January 30, 2012

Table 1. Experimental and B3LYP Calculated Bond Distances (Angstroms), Angles (degrees), and B3LYP Relative Free Energies (kJ/mol and cm^{-1}) for Compounds 1 and 2

	experimental	calculated singlet	calculated triplet	calculated quintet
compound **1**				
energy		149.5 (12 496 cm^{-1})	0.00	70.5 (5890 cm^{-1})
U1−O	2.518(3)	2.611	2.627	2.587
U1−N1	2.255(4)	2.274	2.282	2.603
U1−N4	2.255(4)	2.276	2.273	2.551
U1−N5	2.253(4)	2.275	2.287	2.274
U1−N81	2.251(4)	2.271	2.280	2.333
U1−C2	2.749(5)	2.770	2.809	3.440
U1−C3	2.774(4)	2.791	2.792	3.417
U1−C6	2.787(5)	2.798	2.798	2.834
U1−C7	2.787(5)	2.774	2.800	2.834
N1−C2	1.432(6)	1.417	1.414	1.351
N4−C3	1.418(6)	1.407	1.415	1.351
C2−C3	1.364(6)	1.394	1.392	1.428
N5−C6	1.419(6)	1.406	1.413	1.423
N81−C7	1.430(6)	1.417	1.415	1.422
C6−C7	1.361(8)	1.394	1.391	1.388
compound **2**				
energy		112.8 (9429 cm^{-1})	0.00	64.6 (5396 cm^{-1})
U−N11	2.198(5)	2.234	2.238	2.523
U−N14	2.224(6)	2.264	2.264	2.523
U-Ct(C_5Me_5)$_{avg}$	2.77 (avg)	2.794 (avg)	2.836 (avg)	2.827
U-Ct(C_5Me_5)$_{avg}$	2.72 (avg)	2.742 (avg)	2.783 (avg)	2.827
U−C12	2.673(7)	2.719	2.726	3.382
U−C13	2.685(8)	2.719	2.724	3.382
N11−C12	1.408(9)	1.409	1.410	1.352
N14−C13	1.42(1)	1.410	1.410	1.352
C12−C13	1.40(1)	1.395	1.393	1.426
N11−U−N14	78.7(2)	77.74	77.77	65.56

(CASSI) were carried out to examine the electronic transitions in both molecules for comparison to experimental absorption data.

EXPERIMENTAL SECTION

All B3LYP[8] (Becke-3 exchange[9] and Lee−Yang−Parr correlation[10] functional) calculations were performed using the Gaussian 09 suite of software.[11] Full geometry optimizations were performed and stationary points characterized via analytical frequency calculations using the Pople double-ζ quality basis set (6-31G(d'))[12] for the C, N, O, and H atoms that contains a polarization (d) function on the C, N, and O atoms and the Stuttgart/Dresden triple-ζ quality basis set (SDD) with an effective core potential (ECP)[13] for the U atom (Table S1, Supporting Information). Solvation calculations were performed with the SMD parametrization[14] of the integral equation formalism variant of the polarizable continuum model (IEFPCM).[15]

Time-dependent DFT (TD-DFT) at the B3LYP-optimized geometry for **2** was performed in Gaussian 09. Triplet−singlet, singlet−triplet, and singlet−singlet excitations were calculated by performing TD-DFT on the triplet-optimized geometry of **2** with the singlet-optimized electronic structure and computing 15 singlet and 15 triplet excitations. Triplet−triplet excitations were calculated by performing TD-DFT on the triplet-optimized geometry with the triplet-optimized electronic structure and computing 15 triplet excitations. The results of the B3LYP TD-DFT calculations can be found in Table S13, Supporting Information.

Highly accurate ab initio calculations by means of the complete active space SCF method (CASSCF)[16] followed by the second-order perturbation theory (CASPT2)[17] approach were used to characterize **1** and **2**. CASSCF/CASPT2 calculations were performed using the MOLCAS-7.7 package.[18] The basis set of the atomic natural orbital type with double-ζ plus polarization quality (ANO-RCC-VDZP) was used for the uranium, nitrogen, and oxygen atoms, whereas a minimal basis set quality (ANO-RCC-MB) was used for the other atoms. Scalar relativistic effects were included using the Douglas−Kroll−Hess Hamiltonian. The computational cost arising from the two-electron integrals was drastically reduced by employing the Cholesky decomposition technique.[19] The decomposition threshold was chosen to be 10^{-4}, as this should correspond to an accuracy in total energies of the order of mHartree or higher. Both compounds belong to the C_1 point group. The experimental geometry of both compounds has been used for the CASSCF/CASPT2 study (Figure S1 and Table S10, Supporting Information) in order to have a snapshot of the molecular electronic structure at the experimental configuration. However, the DFT geometries are in agreement with the experimentally determined values and would most likely give similar electronic properties.

At the CASPT2 level of theory, in order to prevent weak intruder states, an imaginary shift of 0.2 units was added to the external part of the zero-order Hamiltonian. For the two investigated species, at the CASPT2 level, orbitals 1s for C, N, and O atoms and orbitals up to and including 5p for the U atom were kept frozen.

At the CASSCF level, the active space for compound **1** contains 14 electrons distributed in 14 orbitals, CAS(14,14). This active space comprises four π orbitals per ligand as well as two orbitals mainly with f character localized on the uranium atom and four correlating orbitals (almost empty), mainly with mixed f and d character, localized on the uranium atom. Six active electrons come from the uranium atom, corresponding to the valence configuration $5f^3 6d^1 7s^2$, and 8 electrons from the HOMO-1 and HOMO π orbitals of the ligands.

For compound **2**, we made a double choice of active space: (A) the active space contains four electrons distributed among five orbitals, CAS(4,5), and (B) the active space contains eight electrons distributed in eight orbitals, CAS(8,8). The CAS(4,5) (A) consists of two π orbitals on the ligand (π_3 and π_4, LUMO and LUMO+1, respectively)

dx.doi.org/10.1021/ic202522w | Inorg. Chem. 2012, 51, 2058−2064

and three orbitals localized on the U atom with 5f character. The four active electrons are intended to come from the uranium atom. CAS(8,8) (B) can be seen as an expansion of the smaller CAS(4,5) by adding three more orbitals, one mainly containing contribution from the 5f and 6d orbitals of the uranium atom and two π orbitals of the ligand (π_1 and π_2, HOMO-1 and HOMO respectively). The four extra electrons are the ones from the π orbitals of the ligand. We performed the CAS(8,8) calculations only for the lowest singlet, triplet, and quintet spin states; we used this bigger active space as reference for the smaller one. For CAS(4,5) we performed state-average-CASSCF (SA-CASSCF) calculations of several singlet, triplet, and quintet spin states, namely, we computed the six lowest singlet spin states, the three lowest triplet spin states, and the four lowest quintet spin states. The number of states included into the state-average calculations reflects the quasi-degeneracy of few electronic levels within the same spin state. Also, subsequent CASPT2 results were corrected by means of a state-average procedure in order to guarantee the orthogonality of the states involved in the calculations.

The SA-CASSCF/CASPT2 results, based on the CAS(4,5) choice of active space, were followed by CAS-state-interaction (CASSI) analysis as implemented in the MOLCAS-7.7 package. This set of calculations allowed us to evaluate important electronic transitions to be compared to the experimental ones. For the CASSI calculations, SA-CASPT2 energies were included as input instead of the SA-CASSCF energies, since the former contains dynamic correlation and provides more accurate electronic energies. The CASSI results have been corrected also by considering spin−orbit coupling effects.

Electronic absorption spectroscopic measurements were made from 2200 to 250 nm in sealed 1 cm quartz cuvettes with a Jasco V-670 spectrophotometer equipped with a deuterium (D_2) lamp (187−350 nm) and halogen (WI) lamp (330−2700 nm) for both **1** and **2** at ambient temperature in degassed and dried THF.

RESULTS AND DISCUSSION

The electronic structures of complexes **1** and **2** were examined by DFT with the B3LYP exchange-correlation functional.[7,9,10] Calculations were performed on the full molecules for singlet, triplet, and quintet states. Optimized geometries and their relative energies for both compounds in all three states are compared to selected experimental structural parameters in Table 1 (optimized geometries are given in the Supporting Information). The triplet state has the lowest energy and corresponds to a U(IV) f^2 center. There are several low-lying triplet states with different f^2 configurations, and the one reported in Table 1 is the lowest energy one that was found. The singlet corresponds to a closed-shell f^2 state. The quintet corresponds to a ligand to metal charge transfer (LMCT) that results in reduction of the U to an f^3 state with the fourth unpaired electron in a delocalized ligand orbital (doubly occupied HOMO of the triplet, Figures 2 and 3). The triplet structures effectively model the structural details better than the quintet structures and correctly predict the bond distortions observed in the reduced ene−diamide ligands for both species. The quintet structure displays significantly different distances for bonds within the ligands and for the metal−ligand bonds. The structural parameters for the singlet models are very close to the triplet and experimental structures, but this state lies 149.49 and 112.79 kJ/mol (12 496.39 and 9428.51 cm^{-1}) higher in free energy than the triplet for **1** and **2**, respectively. These values are similar to those previously observed both experimentally and using computational methods for related uranium species containing the redox-active ligand dpp-BIAN (dpp-BIAN = 1,2-bis(2,6-diisopropylphenylimino)-acenaphthylene).[3a]

The DFT molecular orbitals for **1** are presented in Figure 2. The two unpaired 5f electrons on U(IV) are spread among

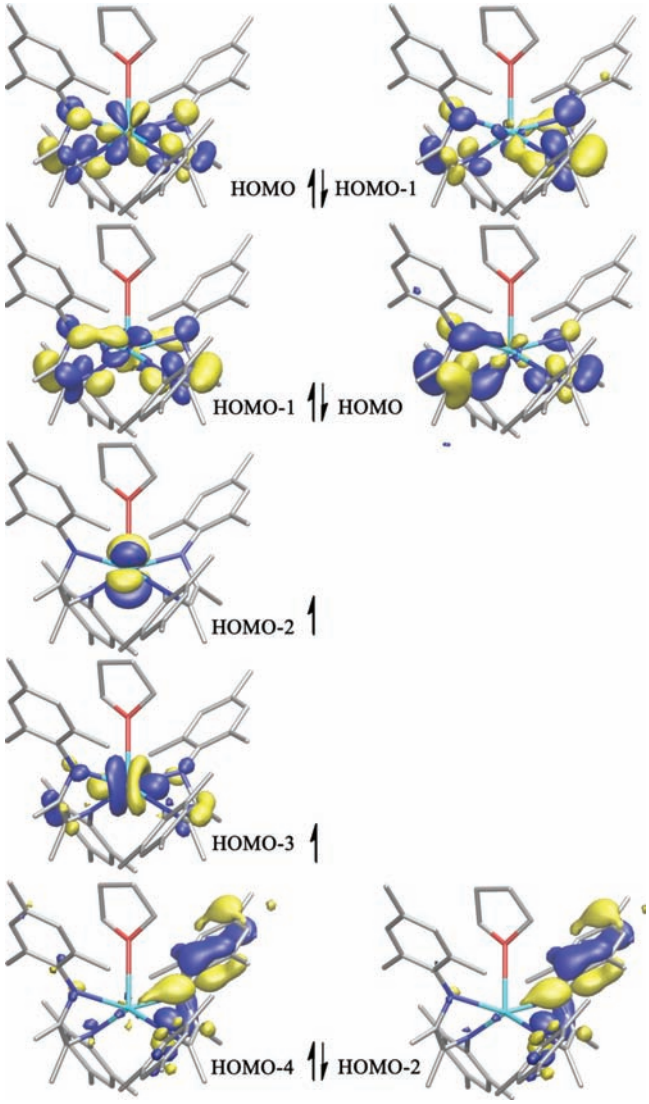

Figure 2. B3LYP molecular orbitals (MOs) for **1**. MOs plotted with an isovalue of 0.05 using VMD.[21] Left column shows the alpha-spin molecular orbitals and the right column shows the beta-spin molecular orbitals. For both spins the orbitals are labeled according to their energetic order among those of the same spin. The orbitals are paired in the Figure next to the closest corresponding orbital of the opposite spin.

several orbitals with one electron being distributed between the HOMO (30% 5f character), the HOMO-1 (12% 5f), and the HOMO-3 (65% 5f) and the second electron being mainly in the HOMO-2 with 88% 5f character. The remainder of these orbitals and the other low-energy orbitals are ligand based, consistent with the observed bond distortions due to ligand reduction. The molecular orbitals presented for **2** in Figure 3 show much less delocalization. The α and β HOMOs are ligand based and clearly illustrate the two-electron reduction of the ligand as expected for U(IV) with a significant amount of nitrogen and carbon 2p character from the ene−diamide ligand and only 18% 5f character. The 5f unpaired electron density is localized in the HOMO-1 and HOMO-2 orbitals with 95% and 86% 5f character, respectively. HOMO-3 also has uranium−diimine ligand character, while HOMO-4 and HOMO-5 are uranium−cyclopentadienyl bonding orbitals. Additional geometry optimizations for singlet and triplet **2** were performed in

dx.doi.org/10.1021/ic202522w | Inorg. Chem. 2012, 51, 2058−2064

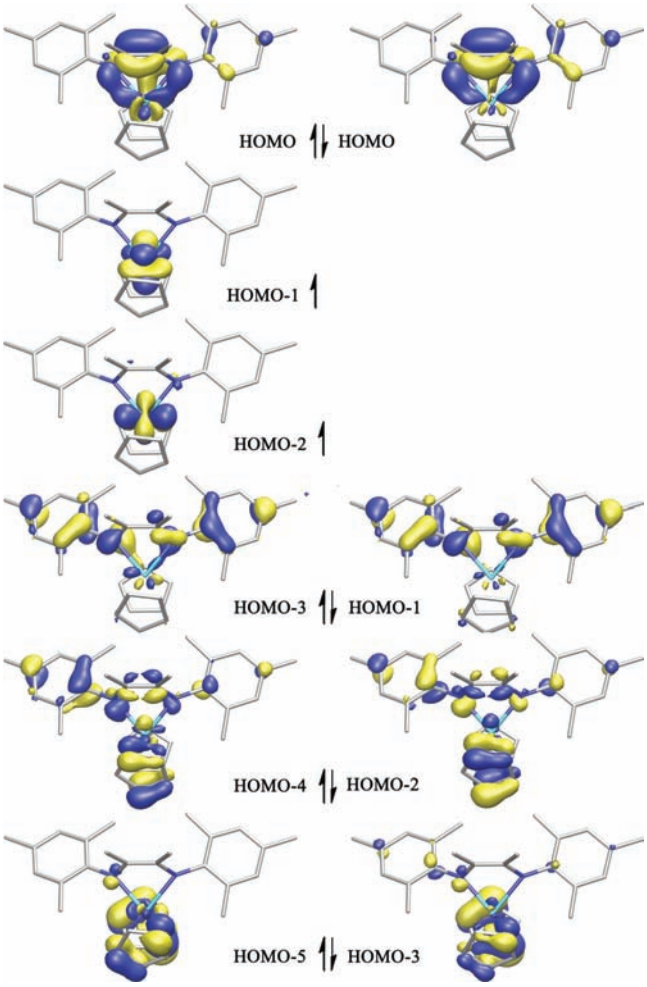

Figure 3. B3LYP molecular orbitals (MOs) for **2**. MOs plotted with an isovalue of 0.05 using VMD.[21] Left column shows the alpha-spin molecular orbitals and the right column shows the beta-spin molecular orbitals. For both spins the orbitals are labeled according to their energetic order among those of the same spin. The orbitals are paired in the Figure next to the closest corresponding orbital of the opposite spin.

THF using the SMD solvation model.[20] The geometric parameters listed in Table 1 changed by less than 0.05 Å and 2°, and the energy difference only increased by 12.0 kJ/mol (1000 cm^{-1}) and 124.8 kJ/mol (10 432 cm^{-1}) in THF and 112.8 kJ/mol (9429 cm^{-1}) in the gas phase, indicating that solvation effects are minimal.

To further elucidate the electronic structures of compounds **1** and **2**, CASSCF/CASPT2 calculations were used. Complexes **1** and **2** have similar electronic structures; consequently, only the details for **2** will be discussed in the main text; those for **1** are presented in the Supporting Information (Figure S2). Results for compound **1** indicate that the triplet spin state is the lowest in energy, with singlet and quintet states lying above it at 63.3 and 436.6 kJ/mol (5292 and 36 497 cm^{-1}), respectively.

The summaries of the energies, main contributions to the multiconfigurational wave function, and occupation numbers of the natural orbitals of the singlet, triplet, and quintet spin states lowest in energy for the CAS(8,8) model of compound **2** are presented in Table 2. The term π_+ is used to denote the linear combination of orbitals $\pi_1 + \pi_2$, and the term π_- denotes the linear combination of orbitals $\pi_1 - \pi_2$, where π_1 represents the bonding combination of the ligand π orbitals with 0 nodes and π_2 represents the bonding combination of the ligand π orbitals with 1 node.

CASPT2 results for compound **2**, based on the CAS(8,8) choice of active space, show that the triplet spin state is the lowest in energy, with singlet and quintet states lying at 47.0 and 211.0 kJ/mol (3930 and 17 640 cm^{-1}) higher in energy, respectively. The absolute CASSCF and CASPT2 energies for the triplet state are −29 289.965124 and −29 292.659234 au, respectively. The triplet spin state is described by a single-determinantal wave function, with two unpaired active electrons distributed in two f orbitals (f_8 and f_9) of the uranium and the remaining 6 active electrons paired in the π_+, π_-, and π_3 orbitals localized on the ligand. Inspection of the CAS wave function for the triplet spin state shows that the configuration $\pi_+^2\pi_-^2\pi_3^2f_8^1f_9^1$ dominates with a weight of 94%. The singlet spin state has an enhanced multiconfigurational character with three closed-shell configurations dominating the optimized CAS wave function, $\pi_+^2\pi_-^2\pi_3^2f_9^2$ (57%), $\pi_+^2\pi_-^2\pi_3^2f_8^2$ (25%), and $\pi_+^2\pi_-^2\pi_3^2f_7^2$ (13%). This mixing of nearly degenerate singlet configurations and its contribution to the second-order perturbation correction to the energy are, in part, responsible for the lower singlet-state energy calculated by CASPT2, as the KS formulation of the DFT does not account for these near-degeneracy issues. Interestingly, the CASSCF singlet−triplet energy difference is quite similar to the DFT difference. The quintet spin state is dominated by the configuration $\pi_+^2\pi_-^2\pi_3^1f_1^1f_3^1f_{13}^1$ with a weight of 93%. DFT calculations

Table 2. Results of the CAS(8,8) Model for Compound 2

	singlet	triplet	quintet
E_{CASSCF} [kJ/mol]	107.3 (8970 cm^{-1})	0.0 (0 cm^{-1})	269.4 (22 520 cm^{-1})
E_{CASPT2} [kJ/mol]	47.0 (3930 cm^{-1})	0.0 (0 cm^{-1})	211.0 (17 640 cm^{-1})
main contributions	$\pi_+^2\pi_-^2\pi_3^2f_9^2$ (57%)	$\pi_+^2\pi_-^2\pi_3^2f_8^1f_9^1$(94%)	$\pi_+^2\pi_-^2\pi_3^1f_1^1f_3^1f_{13}^1$ (93%)
	$\pi_+^2\pi_-^2\pi_3^2f_8^2$ (25%)		
	$\pi_+^2\pi_-^2\pi_3^2f_7^2$ (13%)		
natural orbitals occupation numbers	π_+ (2.00)	π_+ (1.98)	π_+ (1.97)
	π_- (1.98)	π_- (1.98)	π_- (1.93)
	π_3 (1.92)	π_3 (1.92)	π_3 (1.00)
	f_9 (1.21)	f_9 (1.00)	f_1 (1.00)
	f_8 (0.52)	f_8 (1.00)	f_3 (1.00)
	f_7 (0.27)	π_4 (0.09)	f_{13} (1.00)
	π_4 (0.09)	U(5f6d) N(2p) (0.02)	π_4 (0.08)
	U(5f6d)N(2p) (0.02)	U(5f6d) N(2p) (0.02)	U(5f6d)N(2p) (0.02)

dx.doi.org/10.1021/ic202522w | Inorg. Chem. 2012, 51, 2058−2064

predict the triplet−quintet energy difference to be somewhat smaller than that predicted by CASPT2. This difference is due, in part, to the fact that the change in the occupation of the ligand and metal orbitals leads to significant changes in the geometry, which lowers the energy of the quintet, relative to the triplet, while the CASPT2 results are for the vertical excitation energy. The energy lowering of the quintet from the geometry optimization for **2** is 105 kJ/mol (8777 cm^{-1}), and adding this to the optimized DFT energy difference brings the energy difference close to that from the CASPT2. The optimized active natural orbitals of CAS(8,8) for the triplet spin state of **2** are presented in Figure 4 together with the corresponding occupation number. The f orbitals obtained for the singlet and quintet spin states by means of CAS(8,8) are almost identical to the ones obtained with the smaller CAS(4,5) (Figure S3 and Table S11, Supporting Information).

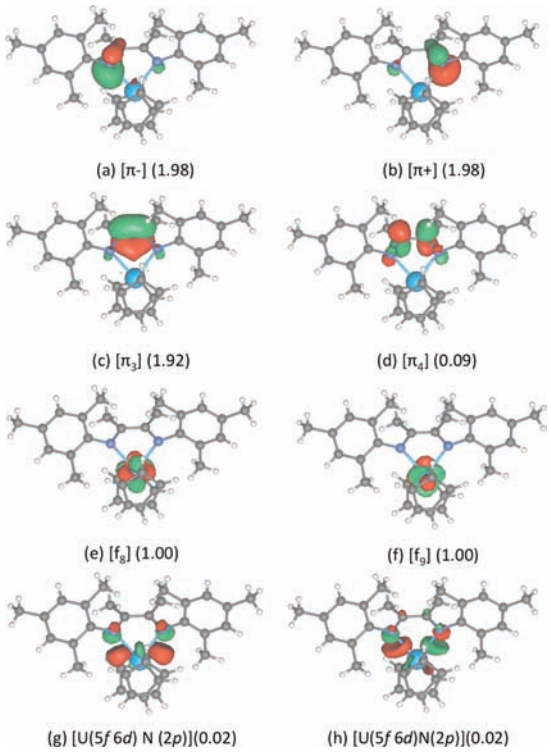

Figure 4. Active molecular orbitals for the CAS(8,8) model of **2** in its ground spin state (triplet). The occupation number for each orbital is given in parentheses. The term π_+ is used to denote the linear combination of orbitals $\pi_1 + \pi_2$, and the term π_- denotes the linear combination of orbitals $\pi_1 - \pi_2$.

For compound **2**, orbitals π_3 and π_4 clearly support the distortions within the ligand framework observed by X-ray crystallography. Orbital π_3 is composed of a π-bonding interaction between the two carbons of the ligand framework. This orbital is almost doubly occupied, with an occupation number of 1.92, and explains the shortening of the carbon−carbon bond experimentally observed. Orbital π_4 has a low occupation number of 0.09 and shows an antibonding interaction between the carbon atoms of the ligand framework, which explains why this carbon−carbon bond does not have full double-bond character (due to π_3) in the observed molecular structure. Further, π_4 depicts the antibonding interaction between the carbon and the nitrogen atoms of the ligand framework. Orbitals f_8 and f_9 are both uranium in character and each occupied by one electron, indicating that these are the location of the unpaired spins.

The SA-CASSCF/CASPT2 calculations for compound **2**, within the CAS(4,5) choice of active space (Table S11, Supporting Information), are consistent with the ones obtained using the CAS(8,8) model. The first three triplet spin states are quasi-degenerate. Preliminary calculations (not presented in this manuscript) showed that the fourth triplet state lies very high in energy (about 400 kJ/mol or 33 440 cm^{-1} above the ground state). These states basically differ in the distribution of two active electrons among the f orbitals of the U atom and the other two located on the π_3 orbital for all the triplet states here analyzed. Analogously, the four optimized quintet spin states differ in the distribution of three unpaired active electrons among f orbitals, the fourth one being always localized in the π_3 orbital of the ligand. The six optimized singlet spin states have mixed contribution of open-shell and closed-shell configurations (Figure S3, Supporting Information). The most relevant CASSI transitions and corresponding oscillator strengths for the above-mentioned states are summarized in Table 3.

For both **1** and **2**, all triplet−triplet transitions are low in energy (since the triplet spin states are quasi-degenerate) with associated energies in the range of 600−1400 cm^{-1} (Figure 5). The triplet−quintet transitions are much higher in energy; they occur at energies greater than 14 000 cm^{-1}. These transitions can be described as ligand-to-metal charge transfer (LMCT) transitions with one electron being excited from the π_3 ligand orbital to the f orbitals of uranium. No other metal-to-ligand charge transfer (MLCT) or ligand-to-metal charge transfer (LMCT) type excitations were observed.

The triplet−singlet transitions occur in an energy range of 5922−10 216 cm^{-1}. Hence, the experimentally observed

Table 3. CASSI Calculated Excitation Energies and Oscillator Strengths for Compound 2

from	to	type	transition (cm^{-1})	transition (nm)	oscillator strength
$\pi_3^2f_1^1f_2^1$	$\pi_3^2f_2^1f_3^1$	T−T	1171	8540	0.9×10^{-5}
$\pi_3^2f_1^1f_2^1$	$\pi_3^2f_1^1f_3^1$	T−T	1437	6959	0.4×10^{-5}
$\pi_3^2f_1^1f_2^1$	$\pi_3^2f_7^2$	T−S_c	8315	1203	0.2×10^{-4}
$\pi_3^2f_1^1f_2^1$	$\pi_3^2f_9^1f_{10}^1$	T−S_o	8450	1183	0.2×10^{-4}
$\pi_3^2f_2^1f_3^1$	$\pi_3^2f_8^1f_9^1$	T−S_o	5927	1687	0.2×10^{-4}
$\pi_3^2f_8^1f_9^1$	$\pi_3^2f_{11}^2$	S_o−S_c	8072	1239	0.3×10^{-3}
$\pi_3^2f_7^2$	$\pi_3^2f_{11}^2$	S_c−S_c	6020	1661	0.4×10^{-3}
$\pi_3^2f_9^1f_{10}^1$	$\pi_3^2f_{11}^2$	S_o−S_c	5853	1709	0.1×10^{-3}
$\pi_3^2f_1^1f_2^1$	$\pi_3^2f_1^1f_4^1f_5^1$	T−Q	15 050	664	0.1×10^{-5}
$\pi_3^2f_1^1f_4^1f_5^1$	$\pi_3^2f_1^1f_3^1f_5^1$	Q−Q	2865	3490	0.1×10^{-3}

dx.doi.org/10.1021/ic202522w | Inorg. Chem. 2012, 51, 2058−2064

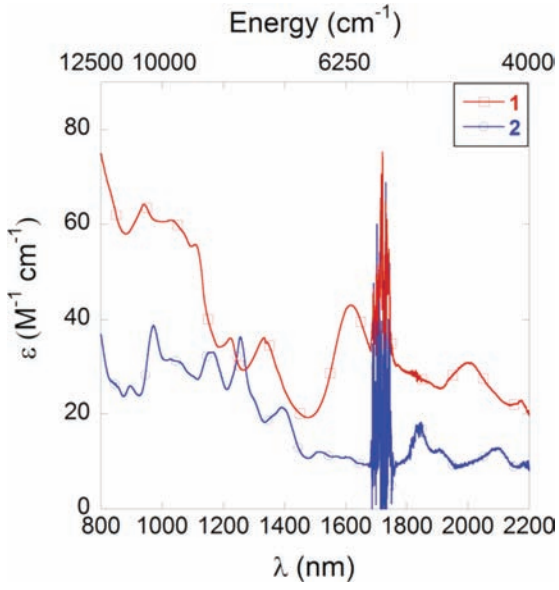

Figure 5. Near-infrared spectra for **1** and **2** recorded in THF at ambient temperature. Solvent overtones present between 1600 and 1800 nm. Both symbols and lines represent experimental data.

transitions are of triplet−singlet type. Also, singlet−singlet transitions appear in a similar range, 4856−8611 cm^{-1}. In order to obtain a deeper understanding of the CT between the ligand and the metal a scan of the excited states higher in energy is required. However, at the experimental level these transitions seem to be masked by intense $\pi_3-\pi_4$ transitions. The CASSI calculations show that only triplet−singlet and singlet−singlet transitions match generally with those that are experimentally observed, with excitations ranging between 4850 cm^{-1} and 10 000 cm^{-1}.

Using the B3LYP-optimized geometry, time-dependent DFT (TD-DFT) was used to further probe the excitation energies of compound **2**. Triplet−singlet, singlet−triplet, and singlet−singlet excitations were calculated by performing TD-DFT calculations at the triplet-optimized geometry of **2** with the singlet-optimized electronic structure and calculating 15 singlet and 15 triplet excitations. Triplet−triplet excitations were calculated by performing TD-DFT calculations at the triplet-optimized geometry with the triplet-optimized electronic structure and calculating 15 triplet excitations. The results of the B3LYP TD-DFT calculations can be found in Table S12, Supporting Information. The multireference counterpart (CASSI) shows that the above-mentioned triplet−triplet transitions occur at lower energy (1437 cm^{-1} at most) and that they exhibit lower oscillator strength (less than 10^{-5}) values as compared to triplet−singlet and singlet−singlet transitions (Table 3).

The CASSI calculations argue that only triplet−singlet and singlet−singlet transitions match those experimentally observed, with excitations energies ranging between 4850 and 10 000 cm^{-1} and oscillator strength values ranging between 10^{-5} and 10^{-4} units. The B3LYP TD-DFT results suggest that some triplet−triplet transitions are also in this range.

In summary, the computational analysis presented supports the reduction of all α-diimine ligands in compounds **1** and **2** by two electrons, which has been demonstrated experimentally.[6] Thus, the ene−diamide resonance form of the ligand is the most accurate representation upon coordination to the uranium center. CASSCF/CASPT2 calculations establish the triplet spin state as being the lowest in energy. It features a tetravalent uranium atom and a dianionic ligand. Two active electrons are localized in the π_3 LUMO orbital of the ligand, which explain the distortion of the C−C bond on the ligand. Geometry optimizations from DFT effectively model the bond distortion of the ligand. Further, results from the CASSI method predicted a general matching between triplet−singlet and singlet−singlet transitions with the experimentally obtained electronic absorption spectra. The triplet−quintet excitations occur at higher energy, and they can be described as LMCT excitations.

■ ASSOCIATED CONTENT

Ⓢ Supporting Information

Computational details. This material is available free of charge via the Internet at http://pubs.acs.org.

■ AUTHOR INFORMATION

Corresponding Author

*E-mail: hall@science.tamu.edu (M.B.H.); gagliard@umn.edu (L.G.); sbart@purdue.edu (S.C.B.).

■ ACKNOWLEDGMENTS

The authors acknowledge financial support from Purdue University and the National Science Foundation (CHE-0541587 to TAMU), the Nuclear Forensics Education Award Program, the U.S. Department of Energy through Grant No. DE-SC002183, and the University of Minnesota Supercomputing Institute.

■ REFERENCES

(1) (a) Bart, S. C.; Lobkovsky, E.; Chirik, P. J. *J. Am. Chem. Soc.* **2004**, *126*, 13794−13807. (b) Blackmore, K. J.; Ziller, J. W.; Heyduk, A. F. *Inorg. Chem.* **2005**, *44*, 5559−5561. (c) Bouwkamp, M. W.; Bowman, A. C.; Lobkovsky, E.; Chirik, P. J. *J. Am. Chem. Soc.* **2006**, *128*, 13340−13341. (d) Smith, A. L.; Hardcastle, K. I.; Soper, J. D. *J. Am. Chem. Soc.* **2010**, *132*, 14358−14360. (e) Benedito, F. L.; Petrenko, T.; Bill, E.; Weyhermueller, T.; Wieghardt, K. *Inorg. Chem.* **2009**, *48*, 10913−10925.

(2) (a) Diaconescu, P. L.; Cummins, C. C. *J. Am. Chem. Soc.* **2002**, *124*, 7660−7661. (b) Evans, W. J.; Nyce, G. W.; Ziller, J. W. *Angew. Chem., Int. Ed.* **2000**, *39*, 240−242. (c) Evans, W. J.; Kozimor, S. A.; Ziller, J. W.; Kaltsoyannis, N. *J. Am. Chem. Soc.* **2004**, *126*, 14533−14547. (d) Diaconescu, P. L.; Arnold, P. L.; Baker, T. A.; Mindiola, D. J.; Cummins, C. C. *J. Am. Chem. Soc.* **2000**, *122*, 6108−6109. (e) Evans, W. J.; Kozimor, S. A.; Ziller, J. W. *Chem. Commun.* **2005**, 4681−4683. (f) Zi, G.; Jia, L.; Werkema, E. L.; Walter, M. D.; Gottfriedsen, J. P.; Andersen, R. A. *Organometallics* **2005**, *24*, 4251−4264. (g) Kraft, S. J.; Fanwick, P. E.; Bart, S. C. *Inorg. Chem.* **2010**, *49*, 1103−1110.

(3) (a) Schelter, E. J.; Wu, R.; Scott, B. L.; Thompson, J. D.; Cantat, T.; John, K. D.; Batista, E. R.; Morris, D. E.; Kiplinger, J. L. *Inorg. Chem.* **2010**, *49*, 924−933. (b) Muresan, N.; Lu, C. C.; Ghosh, M.; Peters, J. C.; Abe, M.; Henling, L. M.; Weyhermüller, T.; Bill, E.; Wieghardt, K. *Inorg. Chem.* **2008**, *47*, 4579−4590. (c) Bart, S. C.; Lobkovsky, E.; Bill, E.; Wieghardt, K.; Chirik, P. J. *Inorg. Chem.* **2007**, *46*, 7055−7063. (d) Korobkov, I.; Gorelsky, S.; Gambarotta, S. *J. Am. Chem. Soc.* **2009**, *131*, 10406−10420.

(4) (a) Hinze, J. *J. Chem. Phys.* **1973**, *59*, 6424−6432. (b) Dalgaard, E.; Jorgensen, P. *J. Chem. Phys.* **1978**, *69*, 3833−3844. (c) Schmidt, M. W.; Gordon, M. S. *Annu. Rev. Phys. Chem.* **1998**, *49*, 233−266.

(5) La Macchia, G.; Li Manni, G.; Todorova, T. K.; Brynda, M.; Aquilante, F.; Roos, B. O.; Gagliardi, L. *Inorg. Chem.* **2010**, *49*, 5216−5222.

(6) Kraft, S. J.; Williams, U. J.; Daly, S. R.; Schelter, E.; Kozimor, S. A.; Boland, K. S.; Kikkawa, J. M.; Forrest, W. P.; Christensen, C. N.; Schwarz, D. E.; Fanwick, P. E.; Clark, D. L.; Conradson, S. D.; Bart, S. C. *Inorg. Chem.* **2011**, *50*, 9838−9848.
(7) (a) Khusniyarov, M. M.; Bill, E.; Weyhermüller, T.; Bothe, E.; Harms, K.; Sundermeyer, J.; Wieghardt, K. *Chem.—Eur. J.* **2008**, *14*, 7608−7622. (b) Bart, S. C.; Hawrelak, E. J.; Lobkovsky, E.; Chirik, P. J. *Organometallics* **2005**, *24*, 5518−5527.
(8) Stephens, P. J.; Devlin, F. J.; Chabalowski, C. F.; Frisch, M. J. *J. Phys. Chem.* **1994**, *98*, 11623−11627.
(9) Becke, A. D. *J. Chem. Phys.* **1993**, *98*, 5648−5652.
(10) Lee, C.; Yang, W.; Parr, R. G. *Phys. Rev. B* **1988**, *37*, 785−789.
(11) Frisch, M. J.; Trucks, G. W.; Schlegel, H. B.; Scuseria, G. E.; Robb, M. A.; Cheeseman, J. R.; Scalmani, G.; Barone, V.; Mennucci, B.; Petersson, G. A.; Nakatsuji, H.; Caricato, M.; Li, X.; Hratchian, H. P.; Izmaylov, A. F.; Bloino, J.; Zheng, G.; Sonnenberg, J. L.; Hada, M.; Ehara, M.; Toyota, K.; Fukuda, R.; Hasegawa, J.; Ishida, M.; Nakajima, T.; Honda, Y.; Kitao, O.; Nakai, H.; Vreven, T.; Montgomery, J. A., Jr.; Peralta, J. E.; Ogliaro, F.; Bearpark, M.; Heyd, J. J.; Brothers, E.; Kudin, K. N.; Staroverov, V. N.; Kobayashi, R.; Normand, J.; Raghavachari, K.; Rendell, A.; Burant, J. C.; Iyengar, S. S.; Tomasi, J.; Cossi, M.; Rega, N.; Millam, J. M.; Klene, M.; Knox, J. E.; Cross, J. B.; Bakken, V.; Adamo, C.; Jaramillo, J.; Gomperts, R.; Stratmann, R. E.; Yazyev, O.; Austin, A. J.; Cammi, R.; Pomelli, C.; Ochterski, J. W.; Martin, R. L.; Morokuma, K.; Zakrzewski, V. G.; Voth, G. A.; Salvador, P.; Dannenberg, J. J.; Dapprich, S.; Daniels, A. D.; Farkas, O.; Foresman, J. B.; Ortiz, J. V.; Cioslowski, J.; , Fox, D. J. *Gaussian 09*, Revision B.01; Gaussian, Inc.: Wallingford, CT, 2009.
(12) (a) Hehre, W. J.; Ditchfield, R.; Pople, J. A. *J. Chem. Phys.* **1972**, *56*, 2257−2261. (b) McLean, A. D.; Chandler, G. S. *J. Chem. Phys.* **1980**, *72*, 5639−5648. (c) Frisch, M. J.; Pople, J. A.; Binkley, J. S. *J. Chem. Phys.* **1984**, *80*, 3265−3269. (d) Polarization function exponents are taken from the 6-311G(d) basis set.
(13) Kuechle, W.; Dolg, M.; Stoll, H.; Preuss, H. *J. Chem. Phys.* **1994**, *100*, 7535−7542.
(14) Marenich, A. V.; Cramer, C. J.; Truhlar, D. G. *J. Phys. Chem. B* **2009**, *113*, 6378−6396.
(15) Tomasi, J.; Mennucci, B.; Cammi, R. *Chem. Rev.* **2005**, *105*, 2999−3094.
(16) Roos, B. O.; Taylor, P. R.; Siegbahn, P. E. M. *Chem. Phys.* **1980**, *48*, 157−173.
(17) (a) Andersson, K.; Malmqvist, P.-A.; Roos, B. O.; Sadlej, A. J.; Wolinski, K. *J. Phys. Chem.* **1990**, *94*, 5483−5488. (b) Andersson, K.; Malmqvist, P.-A.; Roos, B. O. *J. Chem. Phys.* **1992**, *96*, 1218−1226.
(18) Aquilante, F.; De Vico, L.; Ferré, N.; Ghigo, G.; Malmqvist, P.-A.; Neogrády, P.; Pedersen, T. B.; Pitonak, M.; Reiher, M.; Roos, B. O.; Serrano-Andrés, L.; Urban, M.; Veryazov, V.; Lindh, R. *J. Comput. Chem.* **2010**, *31*, 224−247.
(19) Aquilante, F.; Pedersen, T. B.; Lindh, R.; Roos, B. O.; Sánchez de Merás, A.; Koch, H. *J. Chem. Phys.* **2008**, *129*, 024113−024120.
(20) Marenich, A. V.; Cramer, C. J.; Truhlar, D. G. *J. Phys. Chem. B* **2009**, *113*, 6378−6396.
(21) Humphrey, W.; Dalke, A.; Schulten, K. *J. Mol. Graphics* **1996**, *14*, 33−38.